

Article

Effects of B_2O_3 on Viscosity, Structure, and Crystallization of Mold Fluxes for Casting Rare Earth Alloyed Steels

Zeyun Cai, Bo Song *, Longfei Li, Zhen Liu and Xiaokang Cui

School of Metallurgical and Ecological Engineering, University of Science and Technology Beijing, Beijing 100083, China; zexiaoyun@126.com (Z.C.); aifei_0105@126.com (L.L.); liuzhen_ustb@163.com (Z.L.); cuixiaokang126@126.com (X.C.)

* Correspondence: songbo@metall.ustb.edu.cn; Tel.: +86-010-62332208

Received: 18 August 2018; Accepted: 14 September 2018; Published: 20 September 2018



Abstract: Amounts of rare earth oxides were transferred into mold fluxes for the continuous casting of rare earth alloyed heavy railway steels. B_2O_3 was added to improve the viscosity properties and the crystallization behavior of this traditional mold flux. Thus, in this paper, effects of B_2O_3 on viscosity, structure, and crystallization of CeO_2 -bearing mold fluxes for casting rare earth alloyed heavy railway steels were investigated by rotating cylinder method, Raman spectroscopy, and magic angle spinning nuclear magnetic resonance (MAS NMR). Experimental results revealed that with the addition of B_2O_3 , viscosity values of mold fluxes at some certain temperatures decreased significantly. By analyzing the structure of glassy mold fluxes, it can be observed that B_2O_3 behaved as a network-forming oxide within the studied system. However, the introduction of the weak bond energy of B–O and the transition from four-fold coordination boron to three-fold coordination boron with loose structural units mainly reduced the viscosity. Moreover, results of X-ray diffraction (XRD) and differential scanning calorimetry (DSC) confirmed that B_2O_3 decreased the crystallization of the crystal phase $Na_4Ca_4(Si_6O_{18})$ and the solidus temperature of mold fluxes. Thus, these results obtained can provide guidelines for designing new mold fluxes for casting rare earth alloyed steels.

Keywords: B_2O_3 ; mold fluxes; viscosity; structure; RE alloyed steels

1. Introduction

Rare earth, as an effective additive, is widely used for the generation of rare earth treated steels and rare earth alloyed steels [1–3], as it can show excellent heat resistance and good weather resistance [4]. However, due to the manufacturing process, rare earth oxides enter mold fluxes and rare earth oxides in some positions were even over 10 wt.%, which has a significant effect on viscosity properties and the crystallization behavior of mold fluxes. Viscosity determines the consumption and the uniform penetration of mold fluxes during continuous casting process, which is directly related to thermal conditions in the meniscus area and the surface quality of casting. Meanwhile, crystallization ability of mold fluxes can control heat transfer and lubrication by changing slag films. When crystallization temperature and crystallization ratio improve, friction between the slab and the mold will increase, leading to the increase of breakout probability.

Wang et al. [5] found that the viscosity of mold fluxes containing over 10 wt.% RE_xO_y was too high to cast smoothly. Qi et al. [6] found that RE_xO_y increased the viscosity of $CaO-Al_2O_3$ based mold fluxes, which needed 14 wt.% Li_2O to balance. Zhang et al. [7] concluded that La_2O_3 increased the crystallization ratio and the film thickness significantly, which was harmful to the casting process. Therefore, viscosity properties and crystallization behavior of mold fluxes for casting rare earth alloyed steels are urgently needed to be studied.

About 5 to 10 wt.% CaF_2 can control the melting temperature, viscosity [8], and heat transfer of traditional mold fluxes since fluoride tends to reduce the polymerization degree of silicate networks and obtain cuspidine [9]. However, part of fluoride compounds are volatilized into the air [10], resulting in air and water pollution. Other parts enter the system of secondary cooling water and rolling, leading to equipment corrosion. Additionally, too much cuspidine generated in slag films between the mold and the shell during casting rare earth alloyed heavy railway steels damages the lubrication and heat transference. It was reported that mold fluxes containing B_2O_3 become a most promising substitute for traditional mold fluxes. B_2O_3 has been taken into consideration for being introduced into mold fluxes to adjust viscosity or crystallization.

Therefore, this work focuses on studying viscosity and crystallization properties of CeO_2 -bearing mold fluxes with different amounts of B_2O_3 . Viscosity tests conclude that B_2O_3 decreases viscosity and the reasonable amount of additive B_2O_3 in mold fluxes is 10 wt.% according to the required viscosity value (0.5 Pa·s at 1300 °C). B_2O_3 decreases the viscosity of the mold fluxes by introducing the weaker bond energy of B–O compared with that of Si–O and the transition from four-fold coordination to three-fold coordination. Crystallization tests indicates that B_2O_3 decreases the crystallization temperature and the solidus temperature of mold fluxes simultaneously. In this paper, results can provide reference for the understanding of developing mold fluxes for casting rare earth alloyed heavy railway steels.

2. Materials and Methods

2.1. Experimental Slags

Reagent grade powders of CaO (≥ 98 wt.%), SiO_2 (≥ 99 wt.%), Al_2O_3 (≥ 99 wt.%), Na_2CO_3 (≥ 99.8 wt.%), B_2O_3 (≥ 98.5 wt.%), and CeO_2 (≥ 99 wt.%) were used as raw materials. CaO was calcined in a muffle furnace at 1000 °C for 10 h and other powders were dried at 500 °C for 5 h to remove moisture and impurities. 3 wt.%, 5 wt.%, 7 wt.% and 10 wt.% B_2O_3 were added into traditional mold fluxes to replace CaF_2 , respectively. Well mixed samples were first ground and pressed into blocks, then melted in a graphite crucible using a silicon molybdenum rod furnace at 1400 °C for 30 min with Ar gas protection. After pre-heating, samples were water quenched and dried at 120 °C for 10 h followed by grinding into powders screened through 200-mesh sieve. Powder samples were subjected to the inductive coupled plasma optical emission spectrometry (ICP-OES) to determine the B_2O_3 content. The chemical composition of experimental mold fluxes analyzed by X-ray fluorescence (XRF) is shown in Table 1, water-quenched slags were homogenous verified by the X-ray diffraction (XRD) analysis in Figure 1.

Table 1. Chemical composition of experimental mold fluxes.

Sample Number	Composition (wt.%)						
	-	CaO	SiO ₂	Al ₂ O ₃	Na ₂ O	B ₂ O ₃	CeO ₂
1	Calculated	27.44	41.46	7.02	13.33	3.00	7.75
	Analyzed	29.77	40.50	6.58	12.58	2.81	7.76
2	Calculated	26.87	40.60	6.88	13.05	5.00	7.60
	Analyzed	29.16	39.71	6.68	12.30	4.63	7.52
3	Calculated	26.31	39.75	6.73	12.78	7.00	7.43
	Analyzed	28.58	38.67	6.48	11.98	6.82	7.47
4	Calculated	25.46	38.46	6.52	12.36	10.00	7.20
	Analyzed	27.88	37.24	6.22	11.66	9.87	7.13

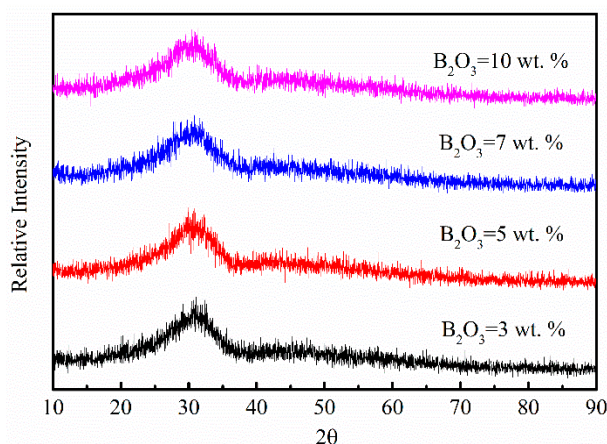


Figure 1. XRD pattern of water quenched slags with different B_2O_3 contents after pre-heating.

2.2. The Viscosity Test

Viscosity values were measured using the rotating cylinder method during decreasing temperature. The measure system had three parts, including a heating system, a rotating system and a measuring system as shown in Figure 2. Resistance furnace (SHIMADEN FP21, Tokyo, Japan) was employed to melt experimental mold fluxes in a molybdenum crucible with the corundum crucible protection. Molybdenum rotor (height of 12 mm and diameter of 15 mm) rotated as the inner cylinder, the measured instrument was a Brookfield DV2T type viscometer (AMETEK Brookfield, Middleboro, MA, USA). Before measurement, viscosity values were calibrated at room temperature (25 °C) by using standard oil with known viscosity (0.495 Pa·s), and the measurement error was less than 2%. The measured viscosity values were calculated via Equation (1):

$$\eta = TK \cdot SMC \cdot \frac{10}{RPM} \cdot \text{Torque} \quad (1)$$

where η is measured viscosity values (Pa·s), TK is the torque constant (0.09373), SMC is the spindle multiplier constant (41.75) and Torque is the practical measured value (10–100%).

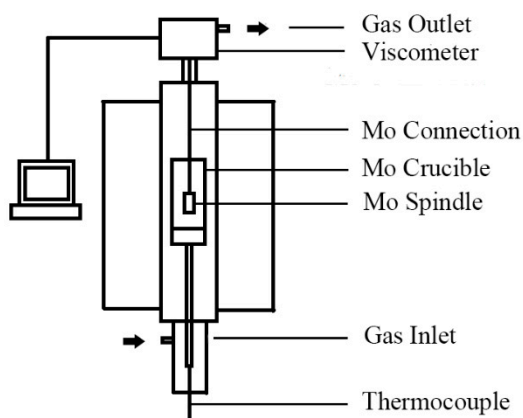


Figure 2. Schematic figure of rotating cylinder viscometer.

Powders (150 g) were put in the molybdenum crucible. Samples were heated at a rate of 10 °C/min from room temperature to 1400 °C in 90% Ar and 10% H_2 atmosphere and held for 30 min. Rotor was used to stir the melts about 15 min before the measurement, and data were automatically recorded by a computer.

2.3. The Structure Test

Raman spectrometry (LabRAM HR Evolution, HORIBA Jobin Yvon S.A.S, Longjumeau, France) was employed to analyze the structure of glassy mold fluxes at room temperature. In this work, the analyzed frequency range was 400–2000 cm^{-1} , and the excitation wavelength was 532 nm. Raman spectra of silicate samples quenched by water are similar to that of melts at high temperature, so it is feasible to study the structure of melts by analyzing the structure of glassy samples.

The ^{11}B MAS NMR spectra of glassy samples were collected on a JNM-ECZ600R spectrometer (14.09 T, JEOL, Tokyo, Japan) at 192.4 MHz, using a probe with 3.2 mm ZrO_2 rotors. ^{11}B MAS spectra were obtained using a single pulse with the frequency of 12 kHz.

2.4. The Crystallization Test

A synchronous thermal analyzer (SDT-Q600, TA, New Castle, DE, USA) was employed to analyze non-isothermal crystallization characteristics of experimental mold fluxes. It can measure heat flow, temperature and weight change simultaneously in the same test condition. About 3 mg powder samples were well mixed and heated in the ZrO_2 crucible at a rate of 20 $^{\circ}\text{C}/\text{min}$ from room temperature to 1300 $^{\circ}\text{C}$ in an Ar atmosphere. All data of differential scanning calorimetry (DSC) were recorded automatically.

An X-ray diffractometer (SMARTLAB 9 kW, Rigaku, Beijing, China) was used to analyze crystal phases of powder samples mentioned as follows. Powder samples were pressed into blocks to melt in a MoSi_2 furnace at a rate of 5 $^{\circ}\text{C}/\text{min}$ from room temperature to the peak temperature on the DSC curve. After holding for 3 h at the peak temperature, samples were air quenched. Then samples were ground and screened to be analyzed using an X-ray diffractometer.

3. Results and Discussion

3.1. Effect of B_2O_3 Content on Viscosity

Figure 3 presents the viscosity of mold fluxes for casting rare earth alloyed heavy railway steels with different B_2O_3 contents. Viscosity continuously decreased and did not have obvious break points with decreasing temperature. The viscosity as function of temperatures decreased with increasing B_2O_3 content, which was more obvious at low temperatures than at high temperatures seen from Figure 3. According to the requirement of a viscosity value of 0.5 Pa·s at 1300 $^{\circ}\text{C}$, the reasonable amount of additive B_2O_3 in mold fluxes for casting rare earth alloyed heavy railway steels is 10 wt.%.

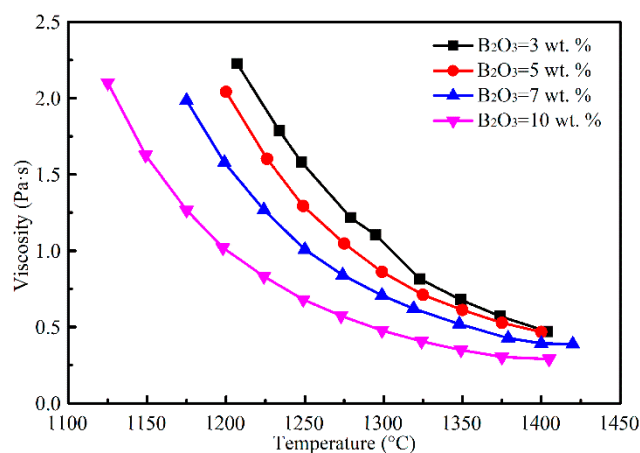


Figure 3. Viscosity results of experimental mold fluxes with decreasing temperature.

Figure 4 presents viscosity results of mold fluxes with different B_2O_3 contents at different temperatures in order to compare their different rheology behaviors. The value of E_a can be obtained as the slope by plotting $\ln \eta$ versus $1/(RT)$ via Equation (2):

$$\ln \eta = \ln A + \frac{E_a}{RT} \quad (2)$$

where η is the viscosity, A is a constant dependent upon the slag structure, E_a is the activation energy of viscosity and R is the gas constant.

The activation energy values of samples are shown in Table 2. The activation energy decreases with increasing B_2O_3 content, which indicates that B_2O_3 decreases the energy barrier and the increase of B_2O_3 is advantageous to the viscous flow.

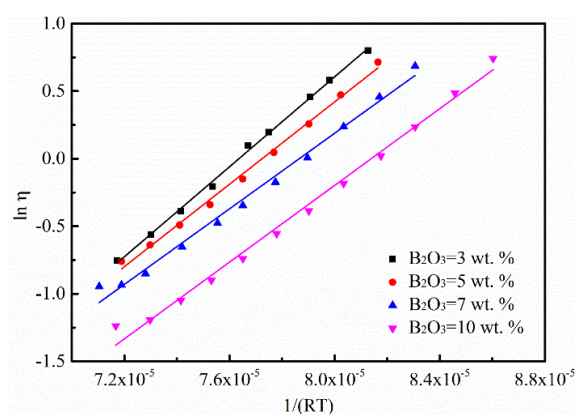


Figure 4. Viscosity results of experimental mold fluxes with decreasing temperature.

Table 2. The activation energy of experimental mold fluxes.

Sample Number	1	2	3	4
E_a (KJ/mol)	166.5 ± 2.7	152.4 ± 3.8	139.9 ± 4.4	142.0 ± 4.0

3.2. The Effect of B_2O_3 Content on Structure

Previous studies [11–13] found that viscosity values at high temperatures could be influenced by network structure and the bond energy of flow units. Raman spectroscopy is one of the techniques which has been widely utilized to analyze the structure of melts. Figure 5 shows the room temperature Raman spectra of mold fluxes with different B_2O_3 contents in this work. For every curve, three Raman peaks mainly appeared around 650 cm^{-1} , 950 cm^{-1} and 1450 cm^{-1} , respectively. With the increasing amount of B_2O_3 , the Raman peak of the band at 950 cm^{-1} was shifted to higher frequencies. The Raman peak of the band at 1450 cm^{-1} could not be observed when the B_2O_3 content was 3 wt.% or 5 wt.%. With continuous increasing B_2O_3 content, relative intensity of the Raman peak of the band at 1450 cm^{-1} increased. The specific explanations about the change of Raman peaks are mentioned in the following sections.

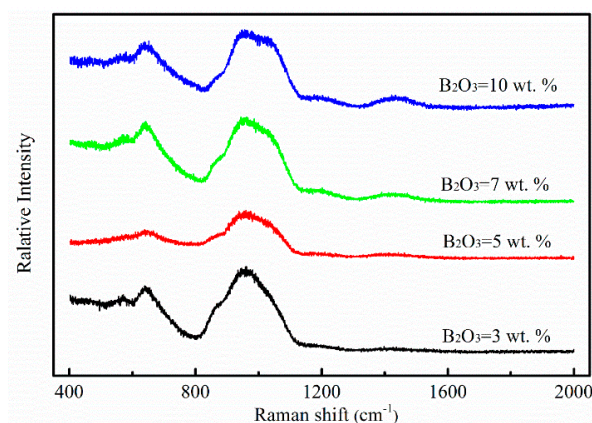


Figure 5. Raman spectra for samples with different B_2O_3 contents at room temperature.

Figure 6a–d show deconvoluted results of the Raman spectra in Figure 5. Raman signals were subtracted and deconvoluted by using a Gaussian-Deconvolution method with the minimum correction coefficient $r^2 \geq 0.995$ [14,15] via Equation (3):

$$I = I_0[1 - \exp(-h\nu/KT)]\nu/(\nu_0 - \nu)^4 \quad (3)$$

where I is the intensity of corrected spectra, I_0 is the intensity of original spectra, ν and ν_0 are frequencies of exciting line and Raman shift, respectively.

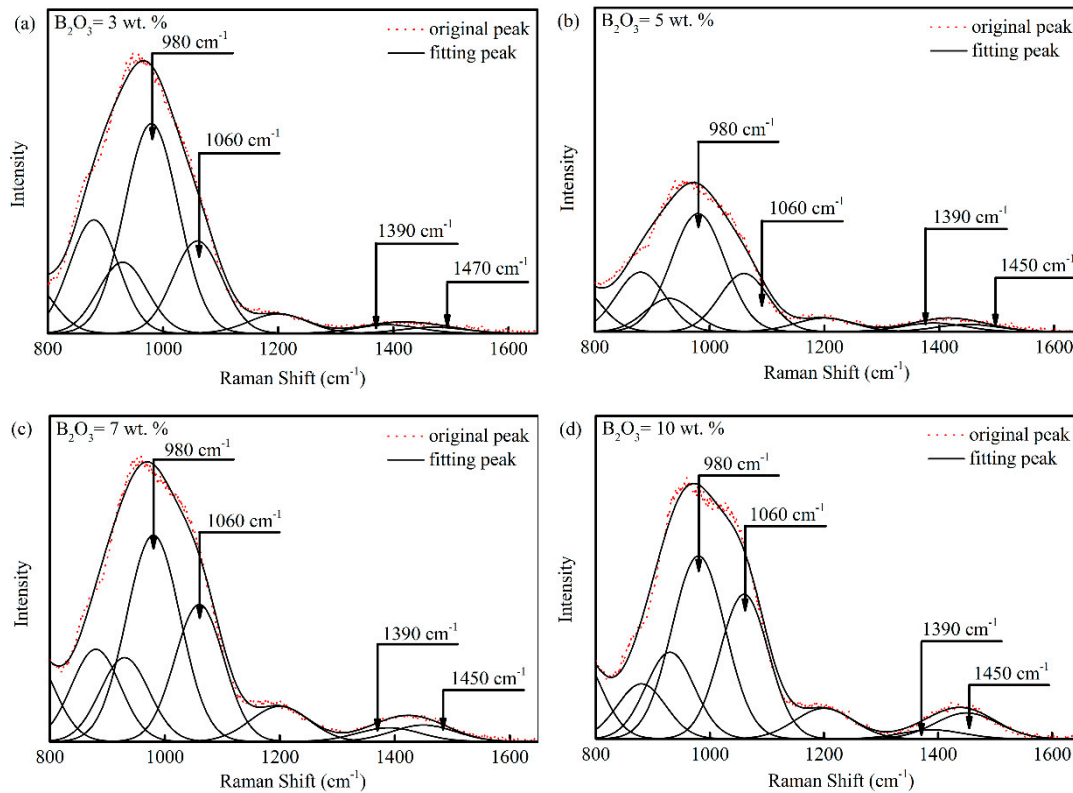


Figure 6. Deconvoluted results of Raman spectra for mold fluxes with different B_2O_3 contents: (a) $B_2O_3 = 3$ wt.%; (b) $B_2O_3 = 5$ wt.%; (c) $B_2O_3 = 7$ wt.% and (d) $B_2O_3 = 10$ wt.%.

In Figure 6a–d, Raman peaks around 980 cm^{-1} and 1060 cm^{-1} are due to the stretching vibration of bridging oxygen in Q_2 and Q_3 structure. Q_2 is $(Si_2O_6)^{4-}$ with two bridging oxygen in single chain structural units and Q_3 is $(Si_4O_{11})^{6-}$ with three bridging oxygen in double chain structural units [16,17]. Peaks around 1390 cm^{-1} and 1450 cm^{-1} are ascribed to BO_2O^- triangles linked to $[BO_4]$ units and BO_2O^- triangles linked to other triangular units [18–20]. The area ratio of a Raman peak is related to the proportion of corresponding structural units in the melt according to Frantz and Mysen [21,22] via Equation (4):

$$X_i = \theta_i \cdot A_i \quad (4)$$

where X_i is the molar fraction, θ_i is the Raman scattering coefficient, A_i is the band area of structure units. It is reasonable to assume that the ratio of Raman scattering coefficients for Q_3 and Q_2 in our system is 2.92 ($\theta_2/\theta_3 = 1/2.92$). It can be obtained from the ratio of X_2 to X_3 in mold fluxes with different B_2O_3 contents. Therefore, the area ratio of Q_2 to Q_3 is estimated and used to represent abundance changes of bridging oxygen. Effects of B_2O_3 on the ratio of Q_2 to Q_3 can be seen in Figure 7, where the estimated ratio of Q_2 to Q_3 decreases with B_2O_3 addition. That means Q_3 increases more quickly than Q_2 , leading to the increase of bridging oxygen in borosilicate glasses. It can be concluded that B_2O_3 plays the role of network former in this system.

Previous studies on the structure of silicates have shown that B_2O_3 can enhance the polymerization as a network former. Furthermore, a certain number of Si–O–B linkages exist in borosilicate and alkaline borosilicate glasses [23,24]. It is proposed that the increase of bridging oxygen may be due to the appearance of Si–O–B units. Normally, the viscosity would increase since structural network became more complex with the addition of B_2O_3 . However, the viscosity of melts is not only decided by the structure, but also the bond energy of structural units. The introduction of B_2O_3 with weak B–O bond energy into silicate with strong Si–O bond energy would lead to the viscosity decrease. Besides, the area of A_1 (peak around 1390 cm^{-1} due to BO_2O^- triangles linked to $[BO_4]$ units) decreased compared with the area of A_2 (BO_2O^- triangles linked to other triangular units) as shown in Figure 8. The area ratio of A_1 to A_2 decreases with increasing B_2O_3 content, which indicates that some BO_2O^- triangles linked to $[BO_4]$ units converted to BO_2O^- triangles linked to other triangular units. In borosilicate melts, there are four-fold coordinated boron and three-fold coordinated boron coexisting. The three-fold coordinated boron is prone to form looser structural units than the four-fold coordinated boron, which is advantageous to the decrease of the viscosity at each temperature in this system.

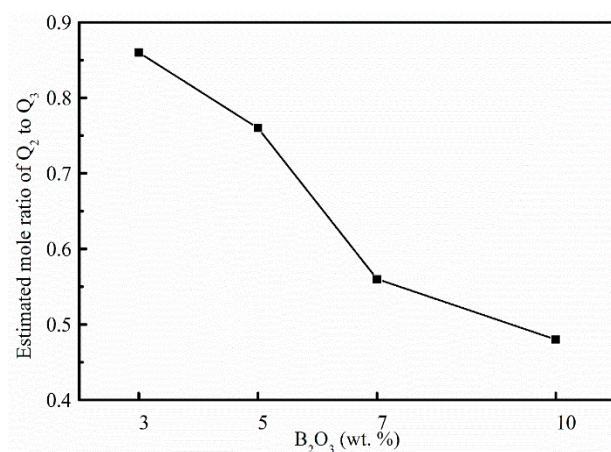


Figure 7. Estimated mole ratio of Q_2 to Q_3 in four experimental mold fluxes.

In this work, although the structure network of mold fluxes became more complex with the increasing B_2O_3 , introduction of B_2O_3 resulted in the decrease of the viscosity at each temperature.

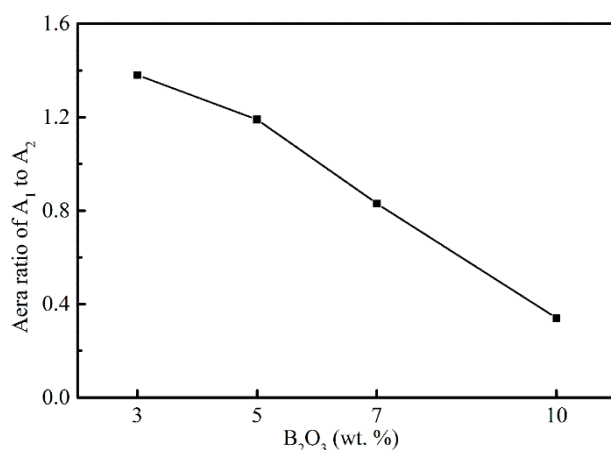


Figure 8. Area ratio of A_1 to A_2 in four experimental mold fluxes.

The signal from $[BO_3]$ and $[BO_4]$ units (centered around 12 ppm and 0 ppm as shown in Figure 9) are well resolved in ^{11}B MAS NMR spectra [25], simultaneously. When the B_2O_3 content increased from 3 to 10 wt.%, the relative intensity of $[BO_3]$ and $[BO_4]$ units both increased. Details about analyses of the spectra are discussed below.

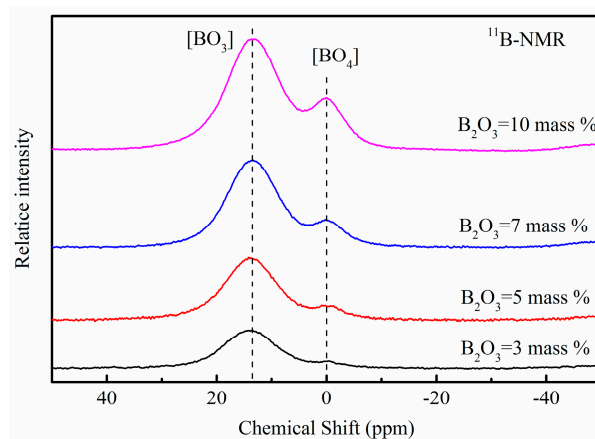


Figure 9. ^{11}B MAS NMR spectra for glassy mold fluxes.

Figure 10a–d show deconvoluted results of MAS NMR spectra in Figure 9. The area ratio of A_3 to A_4 is used to represent the amount ratio of $[\text{BO}_3]$ to $[\text{BO}_4]$ as shown in Figure 11. The area ratio decreases with the addition of B_2O_3 , which is similar to results and analyses of Raman spectra. In conclusion, adding B_2O_3 is of benefit to decrease the viscosity of mold fluxes for casting rare earth alloyed heavy railway steels by changing the structural network.

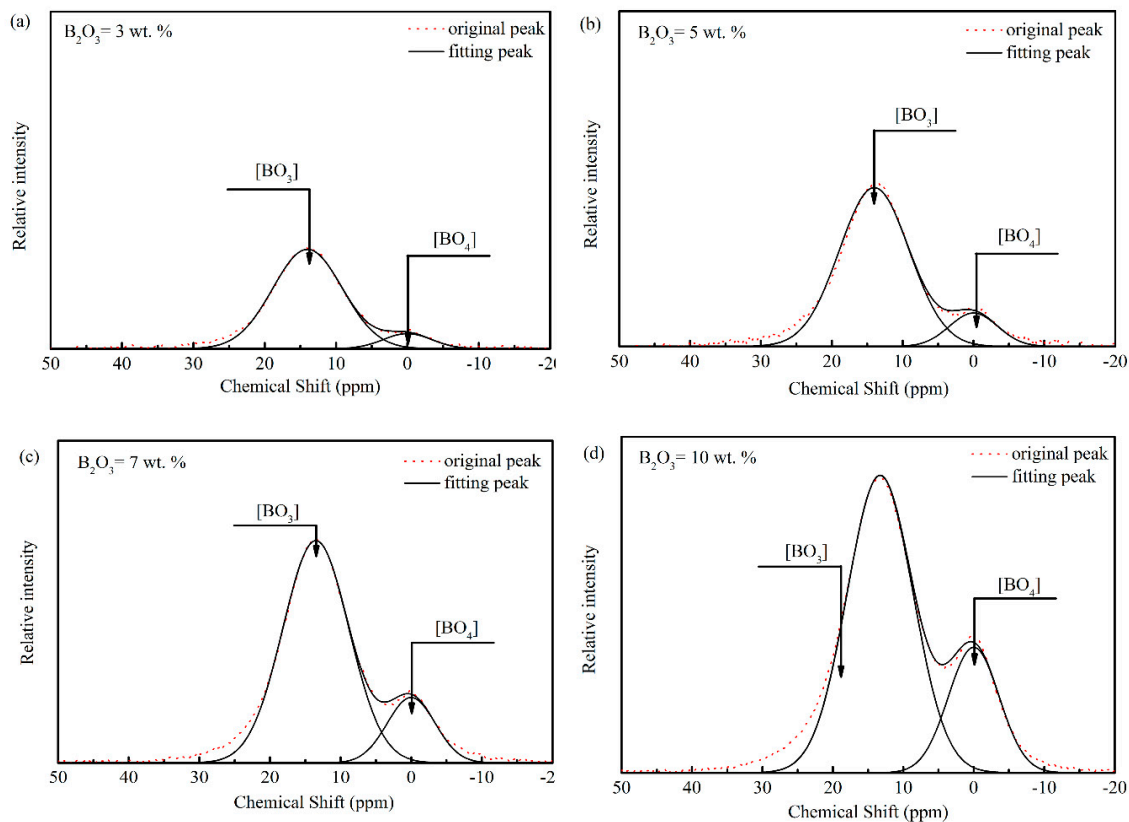


Figure 10. Deconvoluted results of MAS NMR spectra for mold fluxes with different B_2O_3 contents: (a) $\text{B}_2\text{O}_3 = 3$ wt.%, (b) $\text{B}_2\text{O}_3 = 5$ wt.%, (c) $\text{B}_2\text{O}_3 = 7$ wt.%, and (d) $\text{B}_2\text{O}_3 = 10$ wt.%.

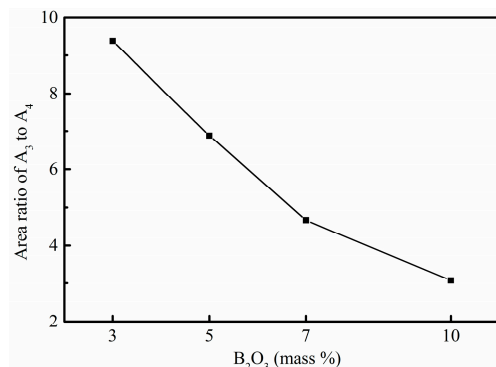


Figure 11. Area ratio of A₃ to A₄ in four experimental mold fluxes.

3.3. Effect of B₂O₃ Content on Crystallization

Figure 12 shows DSC measurements of experimental mold fluxes with 3 wt.%, 5 wt.%, 7 wt.%, and 10 wt.% B₂O₃ during the heating process. With increasing temperature, an exothermic peak appeared around 800 °C, and an endothermic peak appeared about 900 °C, simultaneously. The exothermic peak temperature is referred to as the crystallization temperature of air quenched slags. Its peak area represents the enthalpy of the crystallization associated with the crystallization ability. With the addition of B₂O₃, the exothermic peak became less distinct as shown in Figure 12 corresponding to the decrease of the crystallization ability. Accordingly, the crystalline exothermic peak temperature of mold fluxes for casting rare earth alloyed heavy railway steels decreased first and then increased slightly when B₂O₃ increased from 3 to 10 wt.% as shown in Table 3, which proposes that the crystallization temperature during the heating process decreased first and increased a little later. The endothermic peak temperature is due to the solidus temperature at which the solid phase begins to transit to the liquid phase [26]. When B₂O₃ increased from 3 to 10 wt.%, the solidus temperature of air quenched samples decreased from 911 to 876 °C, as shown in Table 3 since B₂O₃ in mold fluxes has a low melting point or more low-melting compounds appeared. For the experimental mold fluxes, the B₂O₃ addition decreased the crystallization ability and the solidus temperature during the heating process of experimental mold fluxes.

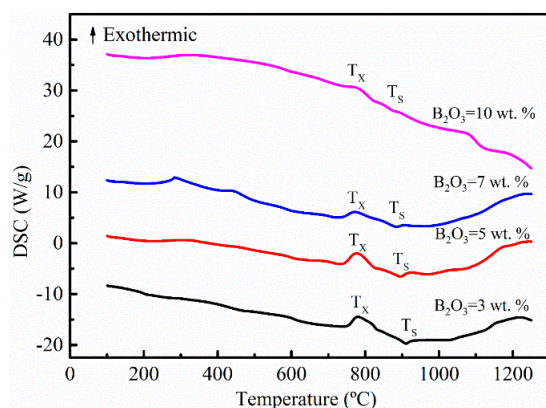


Figure 12. Change of the crystallization temperature (T_x) and the solidus temperature (T_s) in DSC measurements of glass mold fluxes with different B₂O₃ contents at a heat rate of 20 °C/min.

Table 3. Characteristic temperatures of air quenched samples determined by DSC (°C).

Samples	T_x	T_s
1	785	911
2	780	895
3	776	885
4	779	876

Figure 13 presents XRD patterns of air quenched slags after holding for 3 h at the peak temperature of DSC curves. Three kinds of crystal phases were recognized in the samples, such as $\text{Na}_4\text{Ca}_4(\text{Si}_6\text{O}_{18})$, NaAlSiO_4 and $\text{Ca}_2\text{B}_2\text{O}_5$. The relative intensity of $\text{Na}_4\text{Ca}_4(\text{Si}_6\text{O}_{18})$ decreased, but the relative intensity of $\text{Ca}_2\text{B}_2\text{O}_5$ increased with increasing B_2O_3 . It was observed that B_2O_3 was beneficial to the precipitation of $\text{Ca}_2\text{B}_2\text{O}_5$, but not to $\text{Na}_4\text{Ca}_4(\text{Si}_6\text{O}_{18})$. In Figure 12, only one crystalline exothermic peak appeared during the heating process of the four samples, which was attributed to negative conditions of DSC measurements for the secondary crystallization. The exothermic peak of the DSC curves correspond to the crystallization of $\text{Na}_4\text{Ca}_4(\text{Si}_6\text{O}_{18})$ by analyzing the XRD measurements. Thus, B_2O_3 decreases the crystallization temperature and the solidus temperature, and enhances the precipitation of $\text{Ca}_2\text{B}_2\text{O}_5$ instead of $\text{Na}_4\text{Ca}_4(\text{Si}_6\text{O}_{18})$ during the heating process of mold fluxes.

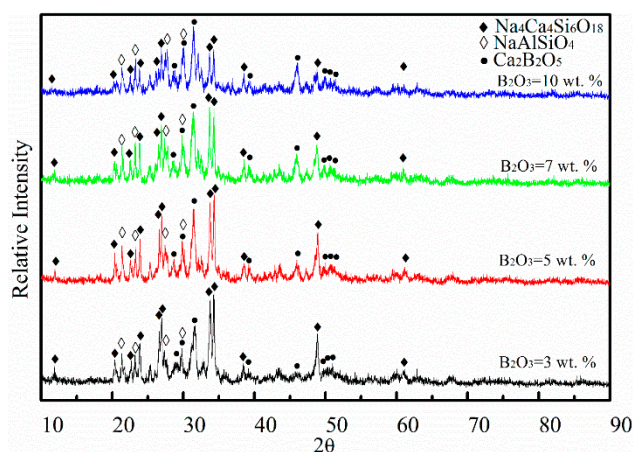


Figure 13. XRD patterns of air quenched samples after heating for 3 h.

4. Conclusions

Viscosity and crystallization of mold fluxes with different B_2O_3 contents ranging from 3 wt.% to 10 wt.% were studied through the rotating cylinder method, DSC, and XRD, and the structure was analyzed using Raman spectra and MAS NMR. Three conclusions are summarized as follows:

1. When B_2O_3 increased from 3 to 10 wt.%, the viscosity and the activation energy of mold fluxes decreased continuously at each temperature, which is beneficial to mold fluxes for casting rare earth alloyed heavy railway steels. According to the requirement of a viscosity value of 0.5 Pa·s at 1300 °C, the reasonable amount of additive B_2O_3 in mold fluxes is 10 wt.%.
2. B_2O_3 played the role of network former in melts, but decreased the viscosity due to the introduction of B–O with weak bond energy and the structural units transition from four-fold coordination boron to threefold coordination boron with loose structure.
3. B_2O_3 decreased the crystallization ability and the melting point by decreasing the crystallization temperature and the solidus temperature of mold fluxes during the heating process. The increase of B_2O_3 was beneficial to the crystallization of $\text{Ca}_2\text{B}_2\text{O}_5$, but not $\text{Na}_4\text{Ca}_4(\text{Si}_6\text{O}_{18})$ during the heating process of mold fluxes.

Author Contributions: Z.C. designed the work and conducted the viscosity experiments and wrote the manuscript under the advice of B.S., B.S., L.L., Z.L. and X.C. revised the manuscript before submission.

Funding: This work was supported by National Natural Science Foundation of China (grant No. 51774024).

Conflicts of Interest: The authors declare no conflict of interest.

References

- Wang, L.M.; Lin, Q.; Ji, J.W.; Lan, D.N. New Study Concerning Development of Application of Rare Earth Metals in Steels. *J. Alloys Compd.* **2006**, *48*, 384–386. [\[CrossRef\]](#)
- Zhou, X.F.; Yin, X.Y.; Fang, F.; Jiang, J.Q.; Zhu, W.L. Influence of Rare Earths on Eutectic Carbides in AISI M2 High Speed Steel. *J. Rare Earths* **2012**, *30*, 1075–1078. [\[CrossRef\]](#)
- Xing, X.G.; Han, Z.J.; Wang, H.F.; Lu, P.N. Electrochemical Corrosion Resistance of CeO₂-Cr/Ti Coatings on 304 Stainless Steel via Pack Cementation. *J. Rare Earths* **2015**, *33*, 1122–1128. [\[CrossRef\]](#)
- Liu, Y.Q.; Wang, L.J.; Chou, K.C. Effect of Cerium on the Cleanliness of Spring Steel Used in Fastener of High-Speed Railway. *J. Rare Earths* **2014**, *32*, 759–766. [\[CrossRef\]](#)
- Wang, D.Y.; Jiang, M.F.; Liu, C.J.; Shi, P.Y.; Yao, Y.; Wang, H.H. Effects of Rare Earth Oxide on Viscosity of Mold Fluxes for Continuous Casting. *J. Rare Earths* **2005**, *23*, 68–72.
- Qi, J.; Liu, C.J.; Li, C.L.; Jiang, M.F. Viscous Properties of New Mold Flux Based on Aluminate System with CeO₂ for Continuous Casting of RE Alloyed Heat Resistant Steel. *J. Rare Earths* **2016**, *34*, 328–335. [\[CrossRef\]](#)
- Zhang, F.; Yuan, C.; Wang, Y.C.; Dong, F.; Wu, M.Q. Influence of La₂O₃ on Crystallization Behavior of Free-fluoride Mold Flux and Heat Transfer of Slag Films. *J. Rare Earths* **2011**, *29*, 173–177. [\[CrossRef\]](#)
- Nichols, M.W.; Lingras, A.P.; Apelian, D. Viscosity Characteristics of Commercial Fluxes for Bottom Poured Ingots. In Proceedings of the Second International Symposium on Metallurgical Slags and Fluxes, Lake Tahoe, NV, USA, 11–14 November 1984; pp. 235–251.
- Seo, M.D.; Shi, C.B.; Baek, J.Y.; Cho, J.W.; Kim, S.H. Kinetics of Isothermal Melt Crystallization in CaO-SiO₂-CaF₂-Based Mold Fluxes. *Metall. Mater. Trans. B* **2015**, *46*, 2374–2383. [\[CrossRef\]](#)
- Zaitsev, A.I.; Leites, A.V.; Lrtvina, A.D.; Mogutnov, B.M. Investigation of the Mould Powder Volatiles During Continuous Casting. *Steel Res. Int.* **1994**, *65*, 368–374. [\[CrossRef\]](#)
- Zhou, L.J.; Wang, W.L.; Zhou, K.C. Viscosity and Crystallization Behavior of F-free Mold Flux for Casting Medium Carbon Steels. *ISIJ Int.* **2015**, *55*, 1916–1924. [\[CrossRef\]](#)
- Shimizu, F.; Tokunaga, H.; Saito, N.; Nakashima, K. Viscosity and Surface Tension Measurements of RE₂O₃-MgO-SiO₂ (RE = Y, Gd, Nd and La) melts. *ISIJ Int.* **2006**, *46*, 388–393. [\[CrossRef\]](#)
- Wang, Z.; Shu, Q.F.; Chou, K.C. Viscosity of Fluoride-free Mold Fluxes Containing B₂O₃ and TiO₂. *Steel Res. Int.* **2013**, *84*, 766–776. [\[CrossRef\]](#)
- Zhang, P.; Grandinetti, P.J.; Stebbins, J.F. Anionic Species Determination in CaSiO₃ Glass using Two-dimensional ²⁹Si NMR. *J. Phys. Chem. B* **1997**, *101*, 4004–4008. [\[CrossRef\]](#)
- Maekawa, H.; Maekawa, T.; Kawamura, K.; Yokokawa, T. The Structural Groups of Alkali Silicate Glasses Determined from ²⁹Si MAS-NMR. *J. Non-Cryst. Solids* **1991**, *127*, 53–64. [\[CrossRef\]](#)
- Sasaki, Y.; Urata, H.; Ishii, K. Structural Analysis of Molten Na₂O-NaF-SiO₂ System by Raman Spectroscopy and Molecular Dynamics Simulation. *ISIJ Int.* **2003**, *43*, 1897–1903. [\[CrossRef\]](#)
- Parkinson, B.G.; Holland, D.; Smith, M.E.; Howes, A.P.; Scales, C.R. The Effect of Oxide Additions on Medium-Range Order Structures in Borosilicate Glasses. *J. Phys. Condens. Matter* **2007**, *19*, 415114. [\[CrossRef\]](#) [\[PubMed\]](#)
- Chrysikos, G.D. Bond Length-Raman Frequency Correlations in Borate Crystals. *J. Raman Spectrosc.* **1991**, *22*, 645–650. [\[CrossRef\]](#)
- Akagi, R.; Ohtori, N.; Umesaki, N. Raman Spectra of K₂O-B₂O₃ Glasses and Melts. *J. Non-Cryst. Solids* **2001**, *293*, 471–476. [\[CrossRef\]](#)
- Chrysikos, G.D.; Kamitsos, E.I.; Patsis, A.P.; Bitsis, M.S.; Karakassides, M.A. The Devitrification of Lithium Metaborate: Polymorphism and Glass Formation. *J. Non-Cryst. Solids* **1990**, *126*, 42–51. [\[CrossRef\]](#)
- Frantza, J.D.; Mysen, B.O. Raman Spectra and Structure of BaO-SiO₂-SrO-SiO₂ and CaO-SiO₂ Melts to 1600 °C. *Chem. Geol.* **1995**, *121*, 155–176. [\[CrossRef\]](#)
- Mysen, B.O.; Frantz, J.D. Structure of Silicate Melts at High Temperature: In-Situ Measurements in the System BaO-SiO₂ to 1669 °C. *Am. Mineral.* **1993**, *78*, 699–709.
- Wang, S.; Stebbins, J.F. Multiple-Quantum Magic-Angle Spinning ¹⁷O NMR Studies of Borate, Borosilicate, and Boroaluminate Glasses. *J. Am. Ceram. Soc.* **1999**, *82*, 1519–1528. [\[CrossRef\]](#)
- Soraru, G.D.; Dallabona, N.; Gervais, C.; Babonneau, F. Organically Modified SiO₂-B₂O₃ Gels Displaying a High Content of Borosiloxane (B-O-Si) Bonds. *Chem. Mater.* **1999**, *11*, 910–919. [\[CrossRef\]](#)

25. Du, L.S.; Stebbins, J.F. Network Connectivity in Aluminoborosilicate Glasses: A High-Resolution ^{11}B , ^{27}Al and ^{17}O NMR Study. *J. Non-Cryst. Solids* **2005**, *351*, 3508–3520. [[CrossRef](#)]
26. Shu, Q.F.; Wang, Z.; Klug, J.L.; Chou, K.C.; Scheller, P.R. Effects of B_2O_3 and TiO_2 on Crystallization Behavior of Slags in Al_2O_3 -CaO-MgO- Na_2O - SiO_2 System. *Steel Res. Int.* **2013**, *84*, 1138. [[CrossRef](#)]



© 2018 by the authors. Licensee MDPI, Basel, Switzerland. This article is an open access article distributed under the terms and conditions of the Creative Commons Attribution (CC BY) license (<http://creativecommons.org/licenses/by/4.0/>).